HHS Public Access

Author manuscript

J Tissue Eng Regen Med. Author manuscript; available in PMC 2021 January 01.

Published in final edited form as:

J Tissue Eng Regen Med. 2020 January ; 14(1): 66–81. doi:10.1002/term.2964.

Synthesis and characterization of osteoinductive visible light-activated adhesive composites with antimicrobial properties

Amirhossein Moghanian[a,b,c,d,*], **Roberto Portillo-Lara**[a,e,*], **Ehsan Shirzaei Sani**[f], **Hailey Konisky**[a], **Seyed Hossein Bassir**[g], **Nasim Annabi**[a,b,c,f,h]

[a]Department of Chemical Engineering, Northeastern University, Boston, MA, 02115-5000, USA

[b]Biomaterials Innovation Research Center, Division of Biomedical Engineering, Department of Medicine, Brigham and Women's Hospital, Harvard Medical School, Cambridge, MA 02139, USA.

[c]Harvard-MIT Division of Health Sciences and Technology, Massachusetts Institute of Technology, Cambridge, MA 02139, USA.

[d]Department of Materials Engineering, Imam Khomeini International University, Qazvin, 34149-16818, Iran.

[e]Tecnologico de Monterrey, Escuela de Ingeniería y Ciencias, Zapopan, JAL 45019, Mexico.

[f]Chemical and Biomolecular Engineering Department, University of California - Los Angeles, Los Angeles, CA 90095, USA.

[g]Department of Periodontology, School of Dental Medicine, Stony Brook University, Stony Brook, NY 11794, USA

[h]Center for Minimally Invasive Therapeutics (C-MIT), California NanoSystems Institute (CNSI), University of California - Los Angeles, Los Angeles, CA 90095, USA

Summary

Orthopedic surgical procedures based on the use of conventional biological graft tissues are often associated with serious post-operative complications such as immune rejection, bacterial infection, and poor osseointegration. Bioresorbable bone grafting substitutes have emerged as attractive alternatives to conventional bone grafting strategies since they can mimic the composition and mechanical properties of the native bone. Among these, bioactive glasses (BGs) hold great potential to be used as biomaterials for bone tissue engineering owing to their biomimetic composition, and high biocompatibility and osteoinductivity. Here, we report the development of a novel composite biomaterial for bone tissue engineering based on the incorporation of a modified strontium (Sr)- and lithium (Li)-doped 58S BG (i.e., BG-5/5) into gelatin methacryloyl (GelMA) hydrogels. We characterized the physicochemical properties of the BG formulation via different analytical techniques. Composite hydrogels were then prepared by directly adding the BG-5/5 formulation to the GelMA hydrogel precursor, followed by photocrosslinking of the polymeric

Corresponding author: N. Annabi, nannabi@ucla.edu.
*These authors contributed equally to this work.

Conflict of interest
The authors declare no conflict of interest.

network via visible light. We characterized the physical, mechanical, and adhesive properties of GelMA/BG-5/5 composites, as well as their *in vitro* cytocompatibility and osteoinductivity. In addition, we evaluated the antimicrobial properties of these composites *in vitro*, using a strain of methicillin-resistant *Staphylococcus Aureus* (MRSA). GelMA/BG-5/5 composites combined the functional characteristics of the inorganic BG component, with the biocompatibility, biodegradability, and biomimetic composition of the hydrogel network. This novel biomaterial could be used for developing osteoinductive scaffolds or implant surface coatings with enhanced osseointegration and intrinsic antimicrobial properties for increased therapeutic efficacy.

Keywords

bioactive glass; antimicrobial; osteoinductive; bioadhesive; orthopedic biomaterials; bone tissue engineering

Introduction

More than two million bone grafts are performed worldwide each year for different surgical procedures in traumatology, orthopedics, oncology, and dentistry (Ho-Shui-Ling et al., 2018). Although biological tissues such as autografts, allografts, and xenografts still constitute the most common sources for bone grafting, they are often hindered by their high cost, limited availability, and other technical limitations (Campana et al., 2014). Furthermore, orthopedic surgical procedures are still largely associated with serious post-operative complications such as hemorrhages, sepsis, immune rejection, and other morbidities (Oryan, Alidadi, Moshiri, & Maffulli, 2014). Because of this, bioresorbable bone grafting substitutes (BGSs) have emerged as attractive alternatives to circumvent the disadvantages associated with conventional approaches for bone augmentation and skeletal repair (Black et al., 2015). In recent years, bone tissue engineering (TE) has emerged as an attractive strategy for the development of BGSs (Ho-Shui-Ling et al., 2018). However, the clinical translation of TE-based approaches is often impaired due to biological safety concerns associated with the use of exogenous growth factors and cells.

Bone is a complex and highly dynamic form of connective tissue that can regenerate and remodel itself through the combined action of different cell types, such as osteoblasts, osteoclasts, and osteocytes. This is mainly because the bone marrow contains a substantial population of mesenchymal stem cells (MSCs) with high osteogenic potential, which can migrate to the site of injury and differentiate to repair the injured tissues (Lin et al., 2017). In addition, bone possesses a highly specialized extracellular matrix (ECM) that heavily influences lineage commitment and stem cell fate (Benders et al., 2013). Because of this, biologically inspired biomaterials have been developed based on the functionalization of implant surfaces and bioengineered scaffolds with ECM-derived biomolecules. Different types of osteoconductive biomaterials, such as hydroxyapatite (HA), calcium phosphates (CaPs), and bioactive glasses (BGs) have been shown to enable the nucleation and growth of CaP crystals both *in vitro* and *in vivo* (Martin & Bettencourt, 2018). Among these, BGs possess comparatively higher bioactivity than HA and CaPs, owing to their high surface reactivity and their ionic dissolution products in aqueous environments (Ciraldo, Boccardi,

Melli, Westhauser, & Boccaccini, 2018). The calcification capacity of these inorganic materials enables the formation of an interfacial layer, which creates a firm bond with the host bone that enhances osseointegration at the implant site (Gkioni, Leeuwenburgh, Douglas, Mikos, & Jansen, 2010). Furthermore, BGs in physiological fluids originate local increases in osmotic pressure and pH due to leaching of ions from the surface, which in turn creates a hostile microenvironment that prevents the growth of a wide range of aerobic and anaerobic bacteria (Drago, Toscano, & Bottagisio, 2018). However, despite the remarkable properties of BGs, their implementation as scaffolding materials for bone TE is limited due to their intrinsic brittleness and low fracture toughness.

Hydrogels are three-dimensional (3D) networks comprised of hydrophilic polymers that are crosslinked to form insoluble matrices with highly tunable physical properties (Bai et al., 2018). Hydrogel-based scaffolds consist of an interconnected macroporous network that promotes the attachment, proliferation, and differentiation of cells. However, due to the biomechanical requirements of osseous tissues, TE scaffolds for orthopedic applications often need to possess high mechanical stiffness to mimic the load bearing properties and functionality of the native bone (Portillo-Lara, Shirzaei Sani, & Annabi, 2017; Shirzaei Sani et al., 2018). The incorporation of inorganic materials into soft hydrogel matrices could be used to enhance their mechanical performance and to deliver bioactive cues that promote scaffold mineralization (Turnbull et al., 2018). Although previous groups have reported the integration of different formulations of BG into highly cytocompatible hydrogels (Negahi Shirazi et al., 2016), the use of toxic crosslinkers or UV light for polymerization has been associated with numerous biosafety concerns (Wang et al., 2015). Here, we aimed to engineer composite hydrogels with intrinsic bioactivity and tunable physicochemical properties, which could help minimize the adverse effects associated with conventional bone grafting strategies. For this, we developed composite hydrogels based on the incorporation of a novel Sr- and lithium (Li)-doped BG (i.e., BG-5/5) into visible light-activated gelatin methacryloyl (GelMA) hydrogels. We characterized the physical, mechanical and adhesive properties, as well as the *in vitro* cytocompatibility, bioactivity and antimicrobial properties of the composites. Our results highlight the remarkable potential of GelMA/BG-5/5 hydrogels for the development of multifunctional scaffolds with intrinsic osteoinductive and antimicrobial properties for bone TE.

Methods

Synthesis of Sr– and Li–doped BG-5/5.

Tetraethylorthosilicate (TEOS: $Si(OC_2H_5)_4$), triethylphosphate (TEP: $PO(OC_2H_5)_3$), calcium nitrate $Ca(NO_3)_2{,}4H_2O$, strontium nitrate $Sr(NO_3)_2$ and lithium nitrate $LiNO_3$ were used as the source for silicon, phosphorus, calcium, strontium, and lithium, respectively. The Sol-Gel method was used to synthesize SiO_2-CaO-P_2O_5-SrO-Li_2O BG with different compositions (Table S1). For the synthesis of 25g $60SiO_2$-26CaO-$4P_2O_5$-5SrO-$5Li_2O$ (mol. %), an acidic media was prepared by mixing 116.96 cm^3 of de-ionized water with 19.50 cm^3 of nitric acid (0.1N) on a magnetic stirrer at 250 rpm for 30 min. To prepare a transparent solution, 53.165 cm^3 of tetraethyl orthosilicate (TEOS) [$SiC_8H_{20}O_4$, Merck] was added to the mixture and stirred for 1 h. After this, 5.4135 cm^3 triethyl phosphate (TEP) [$C_6H_{15}O_4P$,

Merck] were added to the mixture dropwise, and stirred for 1 h. To generate the colloidal solution (Sol), 24.371 g calcium nitrate tetrahydrate [$Ca(NO_3)_2.4H2O$, pure, Merck], 4.200g strontium nitrate [$Sr(NO_3)_2$, Merck] and 2.737g lithium nitrate[$Li(NO_3)$, ≥99%, Sigma-Aldrich] were slowly added to the solution at 45min intervals, for complete dissolution of the nitrate salt. The final mixture was stirred for 1 h, which resulted in a homogenous and transparent Sol. To form the integrated network (gel), the synthesized Sol was poured into a Pyrex container and incubated at 37 °C for 3 days. The gel was then heated to 75°C for 3 days to completely remove residual water, making small holes on the lid of the container to allow the escape of the gases generated by the reaction. Afterwards, the resulting gels were milled in a planetary ball-mill before being stabilized for 3 h at 650 °C with a heating rate of 5 °C/min, to remove the residual nitrate and organic compounds. Lastly, the stabilized powders were cooled down in a furnace at a rate of 5 °C/min.

Analytical and biological characterization of BG-5/5.

Differential thermal analysis (DTA) and thermogravimetric analysis (TGA) of dried gels was carried out using a Shimadzu DSC-50 apparatus to evaluate phase transitions as a function of temperature (from room temperature up to 1,100 °C) in a platinum crucible, under a N_2 atmosphere (50 ml/min) at a constant rate of 10 °C/min. In addition, to analyze changes in phase composition before and after soaking in simulated body fluid (SBF), X-ray diffraction (XRD) (INEL-Equinox-3000, France) was performed on BGs surfaces by applying a Cu Kα X-ray at 40 kV, at a wavelength of 0.15406 nm and in a 2θ range of 20°–50°. In addition, Fourier-transform infrared (FTIR) spectroscopy (Nicolet Avatar 660, Nicolet) was used to evaluate the apatite phase formation on the surface of specimens, using a wavenumber range of 400–4000 cm^{-1}. The disk-shaped BGs were soaked in SBF at 37 °C for 1, 3, 7 and 14 days. The ratio of the sample surface area to the SBF volume was 0.1 cm^2 ml^{-1}. The concentrations of Ca, Si, P, Sr and Li ions in SBF solution were determined via ICP-OES (Varian Vista Pro, Palo Alto, USA), at specific immersion time periods based on chemical changes of the BGs (O'Donnell & Hill, 2010).

To evaluate cell viability and proliferation of MC3T3-E1 cells were seeded on the surface of BG samples, and commercial MTT assays (Sigma) were carried out at days 1, 3 and 7 post-seeding according to instructions from the manufacturer. Osteoblastic activity was evaluated on days 1, 3, and 7 using MC3T3-E1 cells at a density of 1×10^4 cells/cm^2 and a commercial ALP kit (Sigma) according to instructions from the manufacturer. Pristine BG samples, and cells grown in the absence of BG were used as controls.

Synthesis of GelMA/BG-5/5 composites

First, GelMA was prepared by dissolving type A porcine skin gelatin at 10% (w/v) with Dulbecco's phosphate buffered saline (DPBS, GIBCO) at 60 °C (Sani et al., 2019). To form GelMA/BG-5/5 composites, we incorporated both GelMA and BG-5/5 into a single polymeric network using a visible light activated photoinitiator system (Noshadi, Hong, et al., 2017). Briefly, 10% (w/v) GelMA was mixed with a solution containing triethanolamine (TEA, 1.88% (w/v)), N-vinyl caprolactam (VC, 1.25% (w/v)) and Eosin Y disodium salt (0.5 mM). Lastly, varying concentrations of BG-5/5 (1, 5, 10, and 20% (w/v)) were

physically mixed into the precursor solution followed by photocrosslinking of the hydrogels at 100 mW cm^{-2}, using a xenon Genzyme Biosurgery light source (450 to 550 nm).

In vitro swellability, degradation and scanning electron microscopy (SEM) analysis.

Cylindrical GelMA/BGs-5/5 hydrogels (1, 5, 10, and 20% (w/v)) were first formed as described above and lyophilized. The swelling ratio (SR) of the composites was then evaluated by incubating the samples in DPBS at 37 °C for 24 h, and then determining the changes relative to the initial dry weight using the following formula:

$$SR = \frac{W_s - W_0}{W_0}$$

Where W_s and W_0 correspond to the swollen and initial dry weights of the hydrogels, respectively (Noshadi, Hong, et al., 2017). The degradation of the hydrogels was evaluated following incubation in 1 ml DPBS supplemented with 10% FBS at 37 °C for 3 weeks. The percentage degradation at time t (D_t%) was calculated at days 1, 3, 7, 14 and 21, using the following formula:

$$\left(D_t\right) = \frac{W_i - W_t}{W_i} \times 100\%$$

where Wi and Wt correspond to the dry weight before and after incubation for time t, respectively.

The BG particle distribution within the hydrogel network was visualized using a Hitachi S-4800 Scanning Electron Microscope (10kV). For this, the cylindrical GelMA/BG-5/5 samples (7 mm diameter, 2 mm height) were prepared, freeze-dried, and gold/palladium (Au/Pd) coated prior to visualization.

Mechanical characterization.

Hydrogels were synthesized using varying concentrations of BG-5/5 (1, 5, 10, and 20% (w/v)) as described above. An Instron 5542 universal mechanical tester was used to evaluate the mechanical properties of the constructs using standardized tests from the American Society for Testing and Materials (ASTM) (N. Annabi et al., 2017; Noshadi, Hong, et al., 2017). Briefly, polydimethylsiloxane (PDMS) molds were used to form GelMA/BGs compression test samples (cylindrical; diameter: 7 mm, height: 4 mm) as well as tensile samples (rectangular; length: 12.00 mm, width: 5.00 mm, depth: 1.5 mm). For the tensile tests, rectangular GelMA/BGs hydrogels were loaded between two tensile grips and pulled at a rate of 0.5 mm/min until fracture. For compression tests, cylindrical GelMA/BGs were clamped between two compression plates at a compression rate of 0.5 mm/min. Compression modulus was determined as the slope of the linear portion of the stress-strain curve between 0 mm/mm and 0.1 mm/mm compressive strain. Results are reported as average and standard deviation, and at least 4 specimens were analyzed per group.

Adhesive properties.

Hydrogels were synthesized using varying concentrations of BG-5/5 (1, 5, 10, and 20% (w/v)) as described above. The shear strength of the composites was evaluated according to a modified ASTM F2255–05 standard test (Nasim Annabi et al., 2017). Briefly, composites were formed *in situ* by pipetting 10 μl of the precursors between two pieces of gelatin-coated glass slides followed by photocrosslinking via visible light. The hydrogels were then placed between the clamps of the Instron mechanical tester and pulled apart at a strain rate of 10 mm min^{-1}. Shear strength was calculated at the point of detaching. The commercially available sealant Evicel® (Ethicon) was used as a control.

Wound closure was calculated using a modification of the ASTM F2458–05 standard test (Nasim Annabi et al., 2017). For this, porcine bone and skin samples (strips; length: 30.00 mm, width: 10.00 mm, depth: 2 mm) were prepared and glued to glass slides. Hydrogels were placed between the clamps of the Instron machine at a distance of 6 mm. The composites were then photocrosslinked between the tissue samples and the adhesive strength was recorded at the point of tearing at strain rate of 1 mm min^{-1}. The commercially available sealant Evicel® (Ethicon) was used as a control.

In vitro cytocompatibility.

For 2D cell seeding, hydrogels with different concentrations of BG-5/5 (i.e., 1, 5, and 10%) were formed using 8 μl of the precursor solution on TMSPMA-coated slides and photocrosslinked using visible light for 120 sec (Noshadi, Hong, et al., 2017). MC3T3 cells were then seeded on top of the hydrogels at a concentration of 2×10^6 cell/mL and maintained in complete alpha-MEM media. For 3D encapsulation, MC3T3 cells were encapsulated in 8 μL hydrogels on TMSPMA-coated slides at a density of 5×10^6 cell/mL (Noshadi, Walker, et al., 2017).

Cell viability, spreading, and metabolic activity were determined using a commercial LIVE/DEAD assay (Invitrogen), fluorescent f-actin/DAPI staining, and a commercial PrestoBlue kit (Fisher), respectively, at days 1, 3, and 5 (Fares et al., 2018; Soucy et al., 2018). Fluorescent images were acquired using a Zeiss Axio Observer Z1 inverted microscope and analyzed with the ImageJ software (NIH).

Osteogenic differentiation of MC3T3-M1 cells

MC3T3-M1 preosteoblasts were propagated using standard growth media (i.e., α-MEM with nucleosides and no ascorbic acid (Invitrogen), supplemented with 10% FBS (Invitrogen) and 1% penicillin/streptomycin (Invitrogen)). After trypsinization, MC3T3-M1 cells were counted and encapsulated at a density of 4×10^7 cells/mL. Briefly, the hydrogel precursor (with and without the addition of 5% (w/v) BG-5/5) was pipetted directly on top of the pelleted cells and mixed thoroughly to obtain a homogeneous cell suspension. 100 μl of the precursor suspension was sandwiched between two glass slides using two 2-mm spacers, and photocrosslinked as described before. Free-floating cylindrical hydrogels were maintained using three different culture protocols: **a)** 10% (w/v) GelMA hydrogels suspended in standard growth media, **b)** 10% (w/v) GelMA hydrogels suspended in growth media supplemented with 300 ng/mL of BMP-2 (Gibco), and **c)** 10% (w/v) GelMA and 5%

BG-5/5 hydrogels suspended in standard growth media. Cell free GelMA and GelMA/BG hydrogels were also prepared as reference. Hydrogels were maintained in culture for up to 3 weeks, with two intermediate 1-week, and 2-week endpoints.

At the end of each endpoint, hydrogels were carefully harvested, washed thrice with DPBS, and fixed with 4% paraformaldehyde for histological evaluation. For this, 10-μm transversal cryosections were prepared (Noshadi, Walker, et al., 2017) and stained using Alizarin red S staining (Millipore, 2%, pH 4.2) for 2 min, according to instructions from the manufacturer. The differences in the extent of scaffold mineralization were quantitated via threshold analysis of the micrographs using the ImageJ software. In particular, the color threshold was set using cell-free pristine GelMA scaffolds, which were cultured and processed in parallel with cell-laden GelMA and GelMA/BG hydrogels.

Antimicrobial activity.

A LIVE/DEAD® BacLight™ kit (ThermoFisher) was used to determine MRSA cell viability in hydrogels containing 1 and 5% BG-5/5, according to instructions from the manufacturer and following a methodology described in our previous publication (N. Annabi et al., 2017). The samples were imaged using a Zeiss Axio Observer Z1 inverted microscope.

Statistical analysis.

Data were analyzed using either 1- way or 2-way ANOVA tests with the GraphPad Prism 7.0 software. Error was calculated as the mean ± standard deviation (*$p < 0.05$, **$p < 0.01$, and ***$p < 0.001$).

Results

Thermal characterization and X-ray diffraction analysis

Analysis of the DTA (Figure S1a) and TGA (Figure S1b) curves of BG-5/5 showed the first endothermic peak appeared at approximately at 150 °C, which corresponded to the loss of physically adsorbed water in the glass network and ethanol evaporation. The second and third peaks corresponded to the condensation of silanol groups and the elimination of nitrates, which occurred at 390 – 430 °C and 435 – 465 °C, respectively. In addition, exothermic peaks corresponding to the onset of crystallization for BG-5/5 occurred around 1000 °C and 900 °C, respectively.

XRD analysis of BG samples prior to immersion in SBF confirmed its amorphous structure and glassy nature, as demonstrated by the absence of characteristic peaks (Figure S1c). BG-5/5 samples were then immersed in SBF for 1, 3, 7, and 14 days. After 1 day of immersion, the structure of BG surfaces remained amorphous as confirmed by the absence of the corresponding peaks in the XRD patterns (Figure S1c). Diffraction peaks at 25.8 and 31.8 (2θ) corresponded to (200) and (211) atomic planes in the apatite lattice, respectively, according to standard Joint Committee on Powder Diffraction Standards (JCPDS) cards (76–0694). After 3 days of immersion, new peaks appeared at 25.8 and 31.8 for BG-5/5 (Figure S1c). After 7 days of immersion, we observed a slight increase in the intensity of the peaks

corresponding to (200) and (211) for BG-5/5 owing to the increase in apatite formation. This was accompanied with the appearance of a peak at 31.8, which corresponded to (211) atomic planes.

FTIR characterization and evaluation of ion dissolution products

FTIR analysis was conducted in the range of 400–4,000 cm^{-1} with a resolution of 8 cm^{-1} to evaluate apatite formation on the surface of BG-5/5 before and after immersion in SBF. Prior to immersion in SBF, the FTIR spectrum of BG-5/5 specimens revealed characteristic bands corresponding to the silicate network, as demonstrated by the prevalence of SiO_2. Our results showed that all spectra exhibited similar distributions regarding the positions of the different peaks of interest (Figure S1d). For all immersion times, the main infrared bands appeared at 470, 790, 922, 1,066 and 1,250 cm^{-1}, which were related to the Si–O–Si bending vibration, the Si–O symmetric stretching of bridging oxygen atoms between tetrahedrons, Si–O stretching of non-bridging oxygen atoms, Si–O–Si symmetric stretching, and the Si–O– Si asymmetric stretching, respectively (Figure S1d). The band located at 609 cm^{-1} corresponded to the asymmetric vibration of PO_4^{3-} while the stretching mode of the OH group appeared at 3500 and 1651 cm^{-1}. Our results also revealed the appearance of new peaks in the FTIR spectra, which confirmed the formation of apatite on the surface of BG-5/5 at later immersion (Figure S1d). For instance, two additional peaks around 1455 cm^{-1} and 870 cm^{-1} were observed in the FTIR spectra for BG-5/5, which corresponded to C–O stretching in carbonate groups, which were substituted by PO_4^{3-} groups in the apatite lattice after 3 days of immersion in SBF. In addition, the bands corresponding to the P–O absorption appeared as two resolved peaks with increased intensity at 570 and 600 cm^{-1}, which are characteristic of crystalline apatite.

We used ICP-OES analysis to investigate the concentrations of Ca, Si, P, Sr and Li ions, which were released from BG-5/5 throughout different immersion times (i.e., 1, 3, 7, and 14 days) in SBF. Our results showed that the concentration of Ca ions increased rapidly from ≈100 mg/l to ≈290.11 mg/l after 1 day of immersion (Figure S1e), followed by a rapid decrease to ≈124.24 mg/l at day 3. This behavior could be explained in part due to the dissolution and precipitation of Ca ions from the SBF onto the surface of the BG during the crystallization of HA. This observation further confirmed the results obtained from the XRD and FTIR analyses, which showed no peaks indicative of apatite formation after 1 day of immersion in SBF. In addition, ion exchange between Ca, Sr, Li and H, as well as increases in the concentration of Li over time led to an increase in the pH during the first days of immersion (Figure S1f). This was followed by plateau phase up to day 14, owing to the decrease in the soluble Ca concentration in the SBF due to the formation of HA (Figure S1f) (Mozafari, Moztarzadeh, & Tahriri, 2010).

Synthesis and physical characterization of GelMA-BG-5/5 composites.

We first confirmed the cytocompatibility and ALP activity of the base BG-5/5 formulation *in vitro*, using MC3T3-M1 preosteoblasts and standard cytotoxicity and ALP activity assays (Figure S2). Our results demonstrated that cells could proliferate in the presence of the BG formulation (Figure S2a) and that the ALP activity increased consistently up to 7 days of culture (Figure S2b). To form the composites, different concentrations of BG-5/5 (i.e., 1, 5,

10, and 20% (w/v)) were mixed with 10% (w/v) GelMA precursor, followed by photocrosslinking via visible light. We then characterized their physical properties including their porosity, swellability and degradability *in vitro*. First, hydrogel composites were formed using cylindrical molds (7 mm diameter, 2 mm height), freeze dried, and visualized using SEM (Figure 1a–d). SEM micrographs revealed microstructures of irregular and interconnected pores for all samples containing different concentrations of BG-5/5. In addition, the amount of dispersed BG-5/5 particles inside the polymeric network increased at higher BG concentrations. However, hydrogels with 20% (w/v) BG-5/5 exhibited significant particle aggregation, which prevented us from acquiring quality images from these samples and thus, were excluded from this analysis. We then determined the swellability of GelMA/BG-5/5 hydrogels by incubating the composites in Dulbecco's phosphate buffered saline (DPBS) at 37 °C overnight. Our results demonstrated that the swelling ratio of the composites after 24 h increased consistently from 11.78 ± 0.77% to 30.02 ± 1.17% by increasing the concentration of BG-5/5 from 0% to 20%, respectively (Figure 1e). Similarly, our results also showed that the (%) degradation of the composites increased at higher concentrations of BG, from 20.0 ± 0.47% at 0% to 31.43 ± 1.24% at 20%, after 21 days of incubation in DPBS.

Mechanical characterization

Hydrogel composites were synthesized by directly adding varying concentrations of BG-5/5 (i.e., 1, 5, 10, and 20%) to the hydrogel precursors, followed by photocrosslinking via visible light. Our results showed that the compressive modulus of hydrogels increased from 142.49 ± 10.29 kPa to 511.83 ± 32.25 kPa and 757 ± 17.75 kPa when BG-5/5 concentration was enhanced from 0% to 10%, and 20%, respectively (Figure 2b). Our results also showed that the elastic moduli (Figure 2c) and the ultimate tensile strength (Figure 2d) of the composites increased concomitantly by increasing the concentration of BG-5/5. For instance, incorporation of 20% BG-5/5 in GelMA prepolymer increased the elastic modulus of the hydrogels from 122.47 ± 14.37 kPa (pristine GelMA hydrogel) to 383.4 ± 16.11 kPa (composite hydrogel) (Figure 2c), and the ultimate tensile strength from 295.8 ± 10.29 kPa to 394.8 ± 21.01 kPa (Figure 2d). Moreover, although hydrogels synthesized using 10% BG-5/5 exhibited the highest ultimate tensile strength (i.e., 436.69 ± 17.56 kPa), there were no statistically significant differences when compared to hydrogels synthesized using 20% BG-5/5.

In vitro evaluation of tissue adhesive properties

We characterized the adhesive strength of GelMA/BG-5/5 composites to physiological tissues using modified ASTM lap shear (Figure 3a–b) and wound closure (Figure 3c–d) tests. Our results showed that the shear strength of the composites increased consistently by increasing the concentration of BG-5/5 from 0% (i.e., 409 ± 12.97 kPa) to 10% (i.e., 637.1 ± 10.24 kPa) (Figure 3b). However, hydrogels synthesized using 20% BG-5/5 showed comparatively lower shear strength (i.e., 508.78 ± 17.26 kPa). Our results for the wound closure tests showed a similar trend, with consistently higher adhesive strengths to both bone (i.e., 208.7 ± 9.97 kPa, Figure 3c) and skin (i.e., 260.48 ± 15.94 kPa, Figure 3d) for hydrogels synthesized using 10% BG-5/5. Because of this drop in their adhesive properties,

hydrogels containing 20% BG-5/5 were excluded from subsequent experiments involving cell surface seeding and 3D encapsulation.

In vitro evaluation of cytocompatibility

Composite hydrogels were formed in cylindrical molds using 10 % GelMA with 1, 5, and 10% BG-5/5 as describe before, and then seeded with MC3T3 cells at a concentration of 2×10^6 cell/mL and maintained in culture for 5 days (Figure 4). Pristine GelMA hydrogels were used as controls. Cell viability (Figure 4a–h) and spreading (Figure 4i–p) on the composites were then determined via a commercial LIVE/DEAD viability kit and fluorescent F-actin/DAPI staining, respectively. Our results showed that the composites could support the attachment and proliferation of MC3T3-M1 cells, as demonstrated by F-actin/DAPI fluorescent micrographs (Figure 4i–p). In addition, cells remained >90% viable during the first 3 days of culture for all conditions tested, with a slight drop in viability at day 5 post-seeding (Figure 4q). However, despite this relative drop in viability, the metabolic activity of cells increased consistently up to 5 days post-seeding, as demonstrated by a commercial PrestoBlue assay (Figure 4r).

We also evaluated the ability of GelMA/BG-5/5 composites to support the growth and proliferation of 3D -encapsulated MC3T3-M1 cells (Figure 5). For this, cells were mixed with the composite precursors at a density of 5×10^6 cell/mL and photocrosslinked on 3-(trimethoxysilyl) propyl methacrylate (TMSPMA)-coated glass slides. Cell-laden GelMA hydrogels containing 0 (control), 1%, and 5% BG-5/5 were also prepared. Similar to 2D cultures, cell viability (Figure 5a–f) and spreading (Figure 5g–l) on the composites were then determined using a commercial LIVE/DEAD viability kit and fluorescent F-actin/DAPI staining, respectively. Our results showed that overall, cells remained ≈90% viable (Figure 5m) and exhibiting increasingly higher metabolic activity (Figure 5n) up to 5 days post-encapsulation. However, particle aggregation for hydrogels with 10 and 20% (w/v) BG-5/5 prevented the homogeneous distribution of cells and BG particles within the scaffolds and thus, were not used suitable for 3D encapsulation.

In vitro evaluation of osteoinductivity and antimicrobial properties

MC3T3-M1 cells were 3D encapsulated in 10% (w/v) GelMA hydrogels containing 5% (w/v) BG-5/5 and maintained in culture for 1, 2, and 3 weeks. We selected this formulation since it exhibited comparatively better physical, mechanical, and tissue-adhesive properties than hydrogels containing 1% BG-5/5 (w/v). Cells were also encapsulated in pristine GelMA hydrogels with and without BMP-2 supplemented culture media to be used as controls. Visual inspection revealed consistently higher ECM deposition in GelMA/BG composites, as demonstrated by the appearance of mineral crystals on the scaffolds by weeks 2 and 3 post-encapsulation (Figure 6a). Moreover, pristine GelMA hydrogels without BMP-2 supplementation became increasingly softer and structurally weaker, which could be explained in part due to the degradation of the scaffold and the lack of mineralized ECM deposition from encapsulated cells. Histological assessment of the scaffolds using Alizarin Red S (ALP) staining showed that MC3T3-M1 cells in GelMA/BG-5/5 and BMP-2-supplemented GelMA hydrogels exhibited consistently higher levels of calcium deposition, when compared to pristine GelMA controls (Figure 6b). These observations were further

confirmed via quantitative image analysis of the stained micrographs, which demonstrated that GelMA/BG-5/5 composites exhibited significantly higher levels of calcium deposition, when compared to both BMP-2-supplemented and pristine GelMA controls (Figure 6c). In addition, visual inspection also revealed significant differences in scaffold microarchitecture among the experimental conditions tested. Pristine GelMA scaffolds showed large pores and minimal calcium deposition, which correlates to their comparatively weaker structural integrity (Figure 6b). In contrast, both BMP-2-supplemented GelMA and GelMA/BG-5/5 composites exhibited smaller pores and significant calcium deposition, as demonstrated by the higher red coloration in these scaffolds.

For the evaluation of the antimicrobial properties, MRSA bacteria were grown directly on the composites, as well as pristine GelMA hydrogels as controls. For this, we used scaffolds with 1% (w/v)) BG-5/5 as reference, in order to evaluate the differences in antimicrobial properties at lower concentrations of BG. Our results demonstrated that MRSA bacteria could readily colonize pristine GelMA scaffolds, as indicated by the prominent green fluorescence (Figure 6d). In contrast, scaffolds synthesized using 1 (Figure 6e) and 5% (Figure 6f) BG-5/5 exhibited predominant red fluorescence, which was indicative of the bactericidal activity of the composites.

Discussion

Previous studies have reported the development of different BG formulations for biomedical applications, such as BG-58S, BG-68S, and BG-77S (Hench & Jones, 2015; Jones, 2013; Ye, He, Wang, Yao, & Gou, 2014). Among these, BG-58S is one of the most commonly used formulations for bone TE owing to its remarkable biocompatibility and bioactivity (Gong et al., 2014; Ji et al., 2017). Furthermore, the incorporation of bivalent cations to the BG formulation has been shown to enhance the mineralization and vascularization of the scaffold, while also inhibiting the resorption of the newly formed bone (Drago et al., 2018). Among these, Sr ions have been shown to inhibit osteoclast activity, while also promoting the activity of osteoblasts for the formation of new bone (Hoppe & Boccaccini, 2015). Other studies have shown that Sr exhibits mild bactericidal properties at the same concentrations that also up regulate osteoblast activity (Brauer et al., 2013). On the other hand, Li plays a vital role in the proliferation and differentiation of osteoblasts via upregulation of the Wnt pathway, which in turn could enhance osteogenesis and accelerate bone healing *in vivo* (Khorami, Hesaraki, Behnamghader, Nazarian, & Shahrabi, 2011). Furthermore, Li has been shown to enhance bone formation while also possessing immune-stimulating and antimicrobial properties (Kavitha, Subha, ss, & Kulandaivelu, 2014; Miguez-Pacheco et al., 2016). However, although Sr and Li have been used as doping elements in existing formulations of BGs, the simultaneous incorporation of Sr and Li into a SiO_2-CaO-P_2O_5 system has not been explored. We have recently developed and optimized a series of novel BG formulations, among which the formulation consisting of $60SiO_2$-26CaO-$4P_2O_5$-5SrO-$5Li_2O$ (mol. %) (termed BG-5/5) showed the highest cytocompatibility and alkaline phosphatase (ALP) activity (Moghanian, Firoozi, Tahriri, & Sedghi, 2018). Here, we aimed to characterize the physicochemical properties of BG-5/5, as well as the feasibility of incorporating this BG formulation into GelMA hydrogels to yield bioactive and antimicrobial scaffolds for bone repair. For this, we first characterized the

thermal behavior of BG-5/5 (Figure S1a–b). Our results showed that no significant changes were observed above 700 °C, owing to the completion of the chemical reactions and the release of volatile products. Hence, 700 °C was selected as the temperature for stabilization of the BGs.

BGs promote osseointegration through the formation of an interfacial layer of carbonated HA that bonds with the native bone *in vivo*. Moreover, the ionic dissolution products released from BGs under physiological conditions have also been shown to mediate the osteogenic differentiation of stem cells (Hoppe & Boccaccini, 2015). This phenomenon can be evaluated *in vitro* via immersion in an acellular SBF, since it has an ion concentration similar to human plasma. Therefore, we evaluated the ability of BG-5/5 to promote the formation of an interfacial apatite layer in SBF *in vitro* via XRD and FTIR analysis and the evaluation of ion dissolution products. XRD analysis revealed that there was a gradual increase in the intensity of the peaks for the (211) planes from day 7 up to day 14, which was indicative of apatite formation on the surface of the BG (Figure S1c). Furthermore, the maturity of the newly formed apatite layer on the surface of BG-5/5 after 14 days was also demonstrated by the detection of new peaks at 32.18 and 32.86, which corresponded to the crystallization of (112) and (300) atomic planes in the apatite lattice, respectively. The results of the XRD analysis were indicative of the bioactivity of BG-5/5, as demonstrated by the appearance of characteristic peaks at (002) and (211) atomic planes in the apatite lattice at 25.8, 31.8 (2θ°), as well as peaks corresponding to (112) and (300) atomic planes. These results were further confirmed by FTIR spectra (Figure S1d) and the evaluation of ion dissolution products (Figure S1e–f), which further confirmed the formation and the crystallinity of the newly formed HA on BG-5/5 surfaces, following immersion in SBF. We then aimed to form bioactive composite hydrogels by combining BG-5/5 with a highly cytocompatible polymeric network, which could support the attachment and proliferation of progenitor cells that mediate bone repair *in vivo*.

Despite the intrinsic biological activity of BGs, an ideal scaffolding biomaterial should mimic the porosity and interconnected architecture of the native bone, which in turn could promote autologous tissue ingrowth and proper vascularization *in vivo* (Hannink & Arts, 2011). Although the highly hydrophilic nature of hydrogels allows the establishment of a biomimetic microenvironment, excess water-uptake by the hydrogel has been shown to alter its physical properties and impair cell migration and neovascularization (Seeherman & Wozney, 2005). In addition, the scaffolds should be able to be biodegraded at a rate that matches the formation of new tissue, and into nontoxic byproducts that could be readily metabolized by the body. Hence, we evaluated the porous microstructure of GelMA/BG-5/5 composites, as well as their swellability and degradation *in vitro*. SEM analysis revealed the efficient formation of scaffolds comprised of a porous network of GelMA with increasing amounts of dispersed BG-5/5 particles at higher BG concentrations (Figure 1a–d). Our results also showed that increasing the concentration of BG-5/5 led to higher swelling capacity (Figure 1e) and a (%) degradation (Figure 1f) *in vitro*. Taken together, these results suggested that the incorporation of higher concentrations of BG-5/5 into GelMA may reduce the crosslinking density between polymer chains, which may lead to the formation of less compact hydrogel networks with higher water uptake and degradation rates *in vitro*. In contrast, previous groups have reported that the incorporation of different types of

bioceramics into hydrogel-based composites often led to a reduction in pore size and swellability of the scaffold (Killion et al., 2013; Liu et al., 2008; Peter et al., 2010). This characteristic is important since smaller pores and a lower water uptake could impair the cell migration and the adequate colonization of the scaffold.

Collagen and its derivative gelatin have shown great potential for bone TE owing to their ability to promote angiogenesis, wound healing, and osteogenesis *in vivo* (Bai et al., 2018). However, these polymers often exhibit comparatively lower load bearing capacity and elastic moduli, when compared to metallic and ceramic compounds (Turnbull et al., 2018). To address this limitation different types of BGs have been incorporated into ECM-based polymers to produce composite coatings, fillers, or scaffolds with enhanced bioactivity and mechanical performance (Bai et al., 2018; Killion et al., 2013). However, the accurate recapitulation of the physical properties of osseous tissues remains challenging owing to their remarkable mechanical stiffness. For instance, previous groups have reported that the compressive and tensile strength of human cortical bone range between 90 and 230 MPa, and from 90 to 190 MPa, respectively; whereas the compressive strength of trabecular bone ranges between 2 and 45 MPa (Barinov & Komlev, 2011). Therefore, alternative approaches have been explored based on the use of low modulus matrices, which can foster cell proliferation and osteogenic differentiation through bioinspired approaches that drive scaffold mineralization and maturation *in vivo* (Jha, Jackson, & Healy, 2014). The mechanical characterization of GelMA/BG-5/5 composites demonstrated that increasing BG-5/5 concentrations led to consistently higher compressive stress (Figure 2a) and compressive moduli (Figure 2b). Although these observations were in agreement with previous studies which have shown that the mechanical properties of soft polymeric matrices could be increased through the incorporation of inorganic BG fillers (Neumann & Epple, 2006; Sarker, Hum, Nazhat, & Boccaccini, 2015), these values were not in the range of the native bone. However, we envisioned that GelMA/BG-5/5 hydrogels could be used instead to establish a regenerative interfacial niche with the host tissues (Kirkpatrick, 2015). This is mainly because the intrinsic bioactivity of the composites could drive the osteogenic differentiation of migratory MSCs, which in turn could mediate the mineralization and maturation of the scaffold *in vivo* (Huang, Kobayashi, Liu, & Li, 2016). Therefore, although the ability of these composites to be used as load bearing constructs is limited, GelMA-5/5 hydrogels hold remarkable potential to be used as bioactive scaffolds and coating materials that promote bone regeneration and tissue integration *in vivo*.

We then characterized the ability of the composites to bind to physiological tissues, which is directly related to the therapeutic efficacy of the scaffolds and their *in vivo* integration (Figure 3). Our results showed a consistent increase in shear (Figure 3b) and adhesive strength (Figure 3c–d) at higher BG concentrations, up to 10% (w/v). However, although the adhesive strength of 20% BG-5/5 hydrogels was comparatively lower than that of 10% BG-5/5 hydrogels, there were no statistically significant differences between these two conditions. This drop in the adhesive properties and the ultimate tensile strength at 20% BG-5/5 could be explained in part due to the direct interference of BG particles on the formation of the hydrogel network during photocrosslinking. Therefore, we selected the formulations containing 1, 5, and 10% BG-5/5 for subsequent experiments. Furthermore, our results also showed that the adhesive strength of the composites was significantly higher

than the commercially available fibrin-based sealant, Evicel, to both bone (Figure 3c) and skin (Figure 3d) for all BG-5/5 concentrations tested. Taken together, these results highlight the potential of the composites to be used as bioactive adhesive coatings that can be photocrosslinked *in situ* and adhere strongly to the host tissues.

Apart from soluble and insoluble bioactive cues that are present in the physiological microenvironment, the promotion of osteogenic responses depends strongly on the direct interaction of osteoblasts or osteoblast-like cells with the composites. Therefore, we evaluated the cytocompatibility and osteoinductivity of GelMA/BG-5/5 composites via 2D surface seeding (Figure 4) and 3D encapsulation (Figure 5) of MC3T3-M1 preosteoblasts, respectively. Taken together, these results confirmed the *in vitro* cytocompatibility of the composites, as shown by their ability to efficiently support the growth ad proliferation of MC3T3-M1 cells in both 2D and 3D culture conditions. Moreover, these results also showed that the metabolic activity of MC3T3-M1 preosteoblasts increased consistently throughout the duration of the experiment, which was indicative of cells undergoing active replication and protein synthesis (Figure 5n).

BGs provide several technical advantages for bone TE, which are mainly associated with their ability to bind strongly to the native bone, as well as to recruit bone-forming cells that mediate the deposition of osseous ECM components. Hence, we evaluated the ability of the composites to promote the osteogenic differentiation of 3D encapsulated preosteoblasts *in vitro*. Previous groups have demonstrated the ability of growth factors such as bone morphogenetic protein 2 (BMP-2) to induce osteogenic differentiation of MC3T3-M1 cells *in vitro* (Ogasawara et al., 2004). Alternatively, other groups have explored the encapsulation of MC3T3-M1 cells into polymeric hydrogels with embedded bioactive cues such as nanostructured bone-like HA (Demirtas, Irmak, & Gumusderelioglu, 2017), inorganic polyphosphate chains (Wu et al., 2015), and different types of BGs (Marelli et al., 2011; Zeng, Han, Li, & Chang, 2014). Here, we hypothesized that the incorporation of BG-5/5 into GelMA hydrogels could yield a highly cytocompatible matrix with intrinsic osteogenic activity. Histological evaluation confirmed the increased ECM deposition of MC3T3-M1 cells in GelMA/BG-5/5 hydrogels (Figure 6a–c). This approach offers several advantages over conventional approaches based on the delivery of osteogenic growth factors such as BMP-2. For instance, conventional delivery methods often suffer from insufficient local retention and require the use of high protein concentrations to achieve the desired biological effect in larger animal models and humans (Vo, Kasper, & Mikos, 2012). In addition, uncontrolled delivery of growth factors could lead to severe side effects owing to the use of supraphysiological concentrations of these molecules at the target tissue. In contrast, our results demonstrated the intrinsic osteoinductivity of the composites, based on the synergy between the cell-supportive properties of the polymeric GelMA network and the bioactivity of the BG phase.

The development of bioactive scaffolds with antimicrobial properties has gained significant interest since orthopedic implant infections could lead to severe health complications such as septic arthritis and osteomyelitis. Different pathogenic microorganisms, including *Staphylococcus aureus*, *S. epidermidis*, *E. coli* and *P. aeruginosa* have been identified at the site of ≈90% of all orthopedic implants, while also exhibiting varying degrees of resistance

to different antibiotics (Fernandes, Gentile, Pires, Reis, & Hatton, 2017). In recent years, the emergence of antibiotic-resistant strains of pathogenic bacteria has brought forth the need for antibiotic-free strategies to prevent bacterial infections that could lead to orthopedic implant failure. Therefore, local administration of osteoinductive and antimicrobial agents that prevent bacterial infections could represent a more convenient approach following orthopedic procedures. Hence, we then characterized the antimicrobial properties of GelMA/BG-5/5 composites using MRSA as a model organism. Our results demonstrated that the incorporation of increasing concentrations of BG-5/5 led to extensive bacterial death within the composites, as compared to pristine GelMA controls (Figure 6d–f). These results were in agreement with previous studies which have shown that BGs exhibit intrinsic antimicrobial properties owing to the high pH and the osmotic effect caused by their dissolution products. Moreover, the antimicrobial activity of BGs has been demonstrated previously *in vitro* against aerobic and anaerobic pathogens, as well as some strains of antibiotic-resistant bacteria (Lepparanta et al., 2008; Munukka et al., 2008). These results demonstrated the remarkable potential of GelMA/BG-5/5 hydrogels to be used for the treatment of orthopedic infections without the need for local or systemic delivery of antibiotics.

In summary, our results demonstrated that GelMA/BG composites constitute an attractive and cost-effective strategy in the development of osteogenic scaffolds, fillers, orthopedic implant coatings, and other biomedical devices with increased therapeutic efficacy. This is mainly because the composite precursors could be delivered to bone defects of any shape/size and photocrosslinked *in situ* to form an osteoinductive and antimicrobial coating that can adhere to the native bone to promote regeneration of the affected area. These multifunctional composites present various technical advantages over conventional approaches for the treatment and prevention of orthopedic infections. For instance, the intrinsic bioactivity of the scaffolds could promote osteoblastic differentiation of migratory MSCs *in vivo* without the need for high doses of expensive growth factors such as BMP-2. The antimicrobial properties and the high adhesive strength to the native bone could prove remarkably advantageous for the prevention of bacterial infections around orthopedic implants and promotion of osseointegration. In addition, the intrinsic ability of BGs to promote the formation of an interfacial apatite layer could promote osseointegration of the implant, which would in turn increase its therapeutic efficacy. Lastly, the intrinsic angiogenic properties and the high number of cell-binding domains present in gelatin could promote neovascularization at the wound site and enhanced bone repair. Future experiments include the molecular characterization of the pathways involved in osteoblastic differentiation, the characterization of the spectrum of antimicrobial activity with different bacterial strains, integration into biofabrication techniques, and the *in vivo* evaluation of the osteoinductive properties of the scaffold.

Supplementary Material

Refer to Web version on PubMed Central for supplementary material.

Acknowledgments

N.A. acknowledges the support from the American Heart Association (AHA, 16SDG31280010), and National Institutes of Health (NIH) (R01EB023052; R01HL140618), and the startup funds provided by the Department of Chemical and Biomolecular Engineering at UCLA.

References

Annabi N, Rana D, Shirzaei Sani E, Portillo-Lara R, Gifford JL, Fares MM, … Weiss AS (2017). Engineering a sprayable and elastic hydrogel adhesive with antimicrobial properties for wound healing. Biomaterials, 139, 229–243. doi:10.1016/j.biomaterials.2017.05.011 [PubMed: 28579065]

Annabi N, Zhang Y-N, Assmann A, Sani ES, Cheng G, Lassaletta AD, … Wang X (2017). Engineering a highly elastic human protein–based sealant for surgical applications. Science translational medicine, 9(410), eaai7466. [PubMed: 28978753]

Bai X, Gao M, Syed S, Zhuang J, Xu X, & Zhang XQ (2018). Bioactive hydrogels for bone regeneration. Bioact Mater, 3(4), 401–417. doi:10.1016/j.bioactmat.2018.05.006 [PubMed: 30003179]

Barinov SM, & Komlev VS (2011). Calcium phosphate bone cements. Inorganic Materials, 47(13), 1470–1485. doi:10.1134/s0020168511130024

Benders KE, van Weeren PR, Badylak SF, Saris DB, Dhert WJ, & Malda J (2013). Extracellular matrix scaffolds for cartilage and bone regeneration. Trends Biotechnol, 31(3), 169–176. doi:10.1016/j.tibtech.2012.12.004 [PubMed: 23298610]

Black CR, Goriainov V, Gibbs D, Kanczler J, Tare RS, & Oreffo RO (2015). Bone Tissue Engineering. Curr Mol Biol Rep, 1(3), 132–140. doi:10.1007/s40610-015-0022-2 [PubMed: 26618105]

Brauer DS, Karpukhina N, Kedia G, Bhat A, Law RV, Radecka I, & Hill RG (2013). Bactericidal strontium-releasing injectable bone cements based on bioactive glasses. J R Soc Interface, 10(78), 20120647. doi:10.1098/rsif.2012.0647 [PubMed: 23097502]

Campana V, Milano G, Pagano E, Barba M, Cicione C, Salonna G, … Logroscino G (2014). Bone substitutes in orthopaedic surgery: from basic science to clinical practice. J Mater Sci Mater Med, 25(10), 2445–2461. doi:10.1007/s10856-014-5240-2 [PubMed: 24865980]

Ciraldo FE, Boccardi E, Melli V, Westhauser F, & Boccaccini AR (2018). Tackling bioactive glass excessive in vitro bioreactivity: Preconditioning approaches for cell culture tests. Acta Biomater. doi:10.1016/j.actbio.2018.05.019

Demirtas TT, Irmak G, & Gumusderelioglu M (2017). A bioprintable form of chitosan hydrogel for bone tissue engineering. Biofabrication, 9(3), 035003. doi:10.1088/1758-5090/aa7b1d [PubMed: 28639943]

Drago L, Toscano M, & Bottagisio M (2018). Recent Evidence on Bioactive Glass Antimicrobial and Antibiofilm Activity: A Mini-Review. Materials (Basel), 11(2). doi:10.3390/ma11020326

Fares MM, Shirzaei Sani E, Portillo Lara R, Oliveira RB, Khademhosseini A, & Annabi N (2018). Interpenetrating network gelatin methacryloyl (GelMA) and pectin-g-PCL hydrogels with tunable properties for tissue engineering. Biomater Sci, 6(11), 2938–2950. doi:10.1039/c8bm00474a [PubMed: 30246835]

Fernandes JS, Gentile P, Pires RA, Reis RL, & Hatton PV (2017). Multifunctional bioactive glass and glass-ceramic biomaterials with antibacterial properties for repair and regeneration of bone tissue. Acta Biomater, 59, 2–11. doi:10.1016/j.actbio.2017.06.046 [PubMed: 28676434]

Gkioni K, Leeuwenburgh SC, Douglas TE, Mikos AG, & Jansen JA (2010). Mineralization of hydrogels for bone regeneration. Tissue Eng Part B Rev, 16(6), 577–585. doi:10.1089/ten.TEB.2010.0462 [PubMed: 20735319]

Gong W, Huang Z, Dong Y, Gan Y, Li S, Gao X, & Chen X (2014). Ionic extraction of a novel nano-sized bioactive glass enhances differentiation and mineralization of human dental pulp cells. J Endod, 40(1), 83–88. doi:10.1016/j.joen.2013.08.018 [PubMed: 24331996]

Hannink G, & Arts JJ (2011). Bioresorbability, porosity and mechanical strength of bone substitutes: what is optimal for bone regeneration? Injury, 42 Suppl 2, S22–25. doi:10.1016/j.injury.2011.06.008

Hench LL, & Jones JR (2015). Bioactive Glasses: Frontiers and Challenges. Front Bioeng Biotechnol, 3, 194. doi:10.3389/fbioe.2015.00194 [PubMed: 26649290]

Ho-Shui-Ling A, Bolander J, Rustom LE, Johnson AW, Luyten FP, & Picart C (2018). Bone regeneration strategies: Engineered scaffolds, bioactive molecules and stem cells current stage and future perspectives. Biomaterials, 180, 143–162. doi:10.1016/j.biomaterials.2018.07.017 [PubMed: 30036727]

Hoppe A, & Boccaccini AR (2015). Biological Impact of Bioactive Glasses and Their Dissolution Products. Front Oral Biol, 17, 22–32. doi:10.1159/000381690 [PubMed: 26201273]

Huang RL, Kobayashi E, Liu K, & Li Q (2016). Bone Graft Prefabrication Following the In Vivo Bioreactor Principle. EBioMedicine, 12, 43–54. doi:10.1016/j.ebiom.2016.09.016 [PubMed: 27693103]

Jha AK, Jackson WM, & Healy KE (2014). Controlling osteogenic stem cell differentiation via soft bioinspired hydrogels. PLoS One, 9(6), e98640. doi:10.1371/journal.pone.0098640 [PubMed: 24937602]

Ji L, Qiao W, Huang K, Zhang Y, Wu H, Miao S, … Qiu D (2017). Synthesis of nanosized 58S bioactive glass particles by a three-dimensional ordered macroporous carbon template. Mater Sci Eng C Mater Biol Appl, 75, 590–595. doi:10.1016/j.msec.2017.02.107 [PubMed: 28415503]

Jones JR (2013). Review of bioactive glass: from Hench to hybrids. Acta Biomater, 9(1), 4457–4486. doi:10.1016/j.actbio.2012.08.023 [PubMed: 22922331]

Kavitha R, Subha B, ss S, & Kulandaivelu R (2014). Synthesis and Invitro Characterisation of Lithium Doped Bioactive Glass through Quick Alkali Sol-Gel Method (Vol. 1).

Khorami M, Hesaraki S, Behnamghader A, Nazarian H, & Shahrabi S (2011). In vitro bioactivity and biocompatibility of lithium substituted 45S5 bioglass. Materials Science & Engineering C-Materials for Biological Applications, 31(7), 1584–1592. doi:10.1016/j.msec.2011.07.011

Killion JA, Kehoe S, Geever LM, Devine DM, Sheehan E, Boyd D, & Higginbotham CL (2013). Hydrogel/bioactive glass composites for bone regeneration applications: synthesis and characterisation. Mater Sci Eng C Mater Biol Appl, 33(7), 4203–4212. doi:10.1016/j.msec.2013.06.013 [PubMed: 23910334]

Kirkpatrick CJ (2015). Modelling the regenerative niche: a major challenge in biomaterials research. Regen Biomater, 2(4), 267–272. doi:10.1093/rb/rbv018 [PubMed: 26816650]

Lepparanta O, Vaahtio M, Peltola T, Zhang D, Hupa L, Hupa M, … Eerola E (2008). Antibacterial effect of bioactive glasses on clinically important anaerobic bacteria in vitro. J Mater Sci Mater Med, 19(2), 547–551. doi:10.1007/s10856-007-3018-5 [PubMed: 17619981]

Lin W, Xu L, Zwingenberger S, Gibon E, Goodman SB, & Li G (2017). Mesenchymal stem cells homing to improve bone healing. J Orthop Translat, 9, 19–27. doi:10.1016/j.jot.2017.03.002 [PubMed: 29662796]

Liu A, Hong Z, Zhuang X, Chen X, Cui Y, Liu Y, & Jing X (2008). Surface modification of bioactive glass nanoparticles and the mechanical and biological properties of poly(L-lactide) composites. Acta Biomater, 4(4), 1005–1015. doi:10.1016/j.actbio.2008.02.013 [PubMed: 18359672]

Marelli B, Ghezzi CE, Mohn D, Stark WJ, Barralet JE, Boccaccini AR, & Nazhat SN (2011). Accelerated mineralization of dense collagen-nano bioactive glass hybrid gels increases scaffold stiffness and regulates osteoblastic function. Biomaterials, 32(34), 8915–8926. doi:10.1016/j.biomaterials.2011.08.016 [PubMed: 21889796]

Martin V, & Bettencourt A (2018). Bone regeneration: Biomaterials as local delivery systems with improved osteoinductive properties. Mater Sci Eng C Mater Biol Appl, 82, 363–371. doi:10.1016/j.msec.2017.04.038 [PubMed: 29025670]

Miguez-Pacheco V, Buttner T, Macon ALB, Jones JR, Fey T, de Ligny D, … Boccaccini AR (2016). Development and characterization of lithium-releasing silicate bioactive glasses and their scaffolds for bone repair. Journal of Non-Crystalline Solids, 432, 65–72. doi:10.1016/j.jnoncrysol.2015.03.027

Moghanian A, Firoozi S, Tahriri M, & Sedghi A (2018). A comparative study on the in vitro formation of hydroxyapatite, cytotoxicity and antibacterial activity of 58S bioactive glass substituted by Li and Sr. Mater Sci Eng C Mater Biol Appl, 91, 349–360. doi:10.1016/j.msec.2018.05.058 [PubMed: 30033264]

Mozafari M, Moztarzadeh F, & Tahriri M (2010). Investigation of the physico-chemical reactivity of a mesoporous bioactive SiO2-CaO-P2O5 glass in simulated body fluid. Journal of Non-Crystalline Solids, 356(28–30), 1470–1478. doi:10.1016/j.jnoncrysol.2010.04.040

Munukka E, Lepparanta O, Korkeamaki M, Vaahtio M, Peltola T, Zhang D, … Eerola E (2008). Bactericidal effects of bioactive glasses on clinically important aerobic bacteria. J Mater Sci Mater Med, 19(1), 27–32. doi:10.1007/s10856-007-3143-1 [PubMed: 17569007]

Negahi Shirazi A, Fathi A, Suarez FG, Wang Y, Maitz PK, & Dehghani F (2016). A Novel Strategy for Softening Gelatin-Bioactive-Glass Hybrids. ACS Appl Mater Interfaces, 8(3), 1676–1686. doi: 10.1021/acsami.5b09006 [PubMed: 26727696]

Neumann M, & Epple M (2006). Composites of Calcium Phosphate and Polymers as Bone Substitution Materials. European Journal of Trauma, 32(2), 125–131. doi:10.1007/s00068-006-6044-y

Noshadi I, Hong S, Sullivan KE, Shirzaei Sani E, Portillo-Lara R, Tamayol A, … Annabi N (2017). In vitro and in vivo analysis of visible light crosslinkable gelatin methacryloyl (GelMA) hydrogels. Biomater Sci, 5(10), 2093–2105. doi:10.1039/c7bm00110j [PubMed: 28805830]

Noshadi I, Walker BW, Portillo-Lara R, Shirzaei Sani E, Gomes N, Aziziyan MR, & Annabi N (2017). Engineering Biodegradable and Biocompatible Bio-ionic Liquid Conjugated Hydrogels with Tunable Conductivity and Mechanical Properties. Sci Rep, 7(1), 4345. doi:10.1038/s41598-017-04280-w [PubMed: 28659629]

O'Donnell MD, & Hill RG (2010). Influence of strontium and the importance of glass chemistry and structure when designing bioactive glasses for bone regeneration. Acta biomaterialia, 6(7), 2382–2385. doi:10.1016/j.actbio.2010.01.006 [PubMed: 20079468]

Ogasawara T, Kawaguchi H, Jinno S, Hoshi K, Itaka K, Takato T, … Okayama H (2004). Bone morphogenetic protein 2-induced osteoblast differentiation requires Smad-mediated down-regulation of Cdk6. Mol Cell Biol, 24(15), 6560–6568. doi:10.1128/MCB.24.15.6560-6568.2004 [PubMed: 15254224]

Oryan A, Alidadi S, Moshiri A, & Maffulli N (2014). Bone regenerative medicine: classic options, novel strategies, and future directions. J Orthop Surg Res, 9(1), 18. doi:10.1186/1749-799X-9-18 [PubMed: 24628910]

Peter M, Binulal NS, Soumya S, Nair SV, Furuike T, Tamura H, & Jayakumar R (2010). Nanocomposite scaffolds of bioactive glass ceramic nanoparticles disseminated chitosan matrix for tissue engineering applications. Carbohydrate Polymers, 79(2), 284–289. doi:10.1016/j.carbpol.2009.08.001

Portillo-Lara R, Shirzaei Sani E, & Annabi N (2017). Biomimetic Orthopedic Materials. In Li B & Webster T(Eds.), Orthopedic Biomaterials: Advances and Applications (pp. 109–139). Cham: Springer International Publishing.

Sani ES, Kheirkhah A, Rana D, Sun Z, Foulsham W, Sheikhi A, … Annabi N (2019). Sutureless repair of corneal injuries using naturally derived bioadhesive hydrogels. Science Advances, 5, eaav1281. [PubMed: 30906864]

Sarker B, Hum J, Nazhat SN, & Boccaccini AR (2015). Combining collagen and bioactive glasses for bone tissue engineering: a review. Adv Healthc Mater, 4(2), 176–194. doi:10.1002/adhm.201400302 [PubMed: 25116596]

Seeherman H, & Wozney JM (2005). Delivery of bone morphogenetic proteins for orthopedic tissue regeneration. Cytokine Growth Factor Rev, 16(3), 329–345. doi:10.1016/j.cytogfr.2005.05.001 [PubMed: 15936978]

Shirzaei Sani E, Portillo-Lara R, Spencer A, Yu W, Geilich BM, Noshadi I, … Annabi N (2018). Engineering Adhesive and Antimicrobial Hyaluronic Acid/Elastin-like Polypeptide Hybrid Hydrogels for Tissue Engineering Applications. ACS Biomaterials Science & Engineering.

Soucy JR, Shirzaei Sani E, Portillo Lara R, Diaz D, Dias F, Weiss AS, … Annabi N (2018). Photocrosslinkable Gelatin/Tropoelastin Hydrogel Adhesives for Peripheral Nerve Repair. Tissue Eng Part A, 24(17–18), 1393–1405. doi:10.1089/ten.TEA.2017.0502 [PubMed: 29580168]

Turnbull G, Clarke J, Picard F, Riches P, Jia L, Han F, … Shu W (2018). 3D bioactive composite scaffolds for bone tissue engineering. Bioact Mater, 3(3), 278–314. doi:10.1016/j.bioactmat.2017.10.001 [PubMed: 29744467]

Vo TN, Kasper FK, & Mikos AG (2012). Strategies for controlled delivery of growth factors and cells for bone regeneration. Adv Drug Deliv Rev, 64(12), 1292–1309. doi:10.1016/j.addr.2012.01.016 [PubMed: 22342771]

Wang Z, Abdulla R, Parker B, Samanipour R, Ghosh S, & Kim K (2015). A simple and high-resolution stereolithography-based 3D bioprinting system using visible light crosslinkable bioinks. Biofabrication, 7(4), 045009. [PubMed: 26696527]

Wu AT, Aoki T, Sakoda M, Ohta S, Ichimura S, Ito T, … Furukawa KS (2015). Enhancing osteogenic differentiation of MC3T3-E1 cells by immobilizing inorganic polyphosphate onto hyaluronic acid hydrogel. Biomacromolecules, 16(1), 166–173. doi:10.1021/bm501356c [PubMed: 25423088]

Ye J, He J, Wang C, Yao K, & Gou Z (2014). Copper-containing mesoporous bioactive glass coatings on orbital implants for improving drug delivery capacity and antibacterial activity. Biotechnol Lett, 36(5), 961–968. doi:10.1007/s10529-014-1465-x [PubMed: 24563298]

Zeng Q, Han Y, Li H, & Chang J (2014). Bioglass/alginate composite hydrogel beads as cell carriers for bone regeneration. J Biomed Mater Res B Appl Biomater, 102(1), 42–51. doi:10.1002/jbm.b.32978 [PubMed: 23847006]

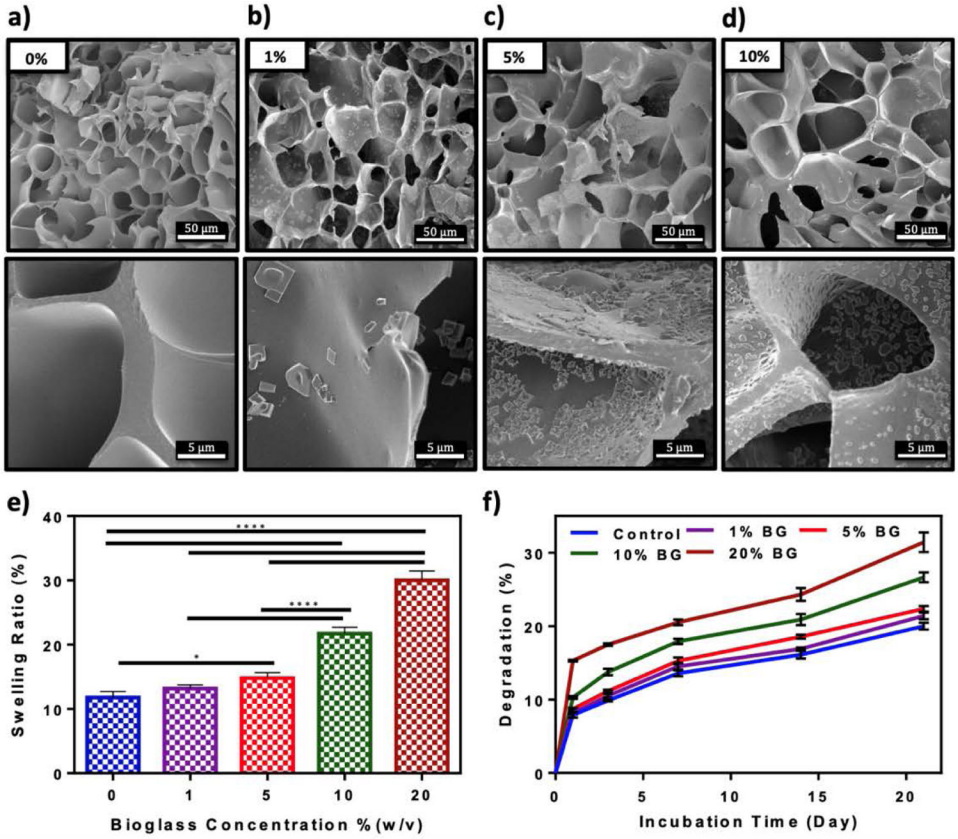

Figure 1. ***In vitro*** **evaluation of porosity, swellability, and degradability of GelMA/BG-5/5 composites.**

Representative SEM images of composites synthesized using 10% (w/v) GelMA and **(a)** 0%, **(b)** 1%, **(c)** 5%, and **(d)** 10% (w/v) BG-5/5 concentrations. **(e)** Swelling ratios and **(f)** degradation rates (change relative to the initial dry weight) of GelMA/BG-5/5 composites incubated in DPBS at 37 °C. Data is represented as mean ± SD (*$p<0.05$, **$p<0.01$, ***$p<0.001$, ****$p<0.0001$ and $n \geq 5$).

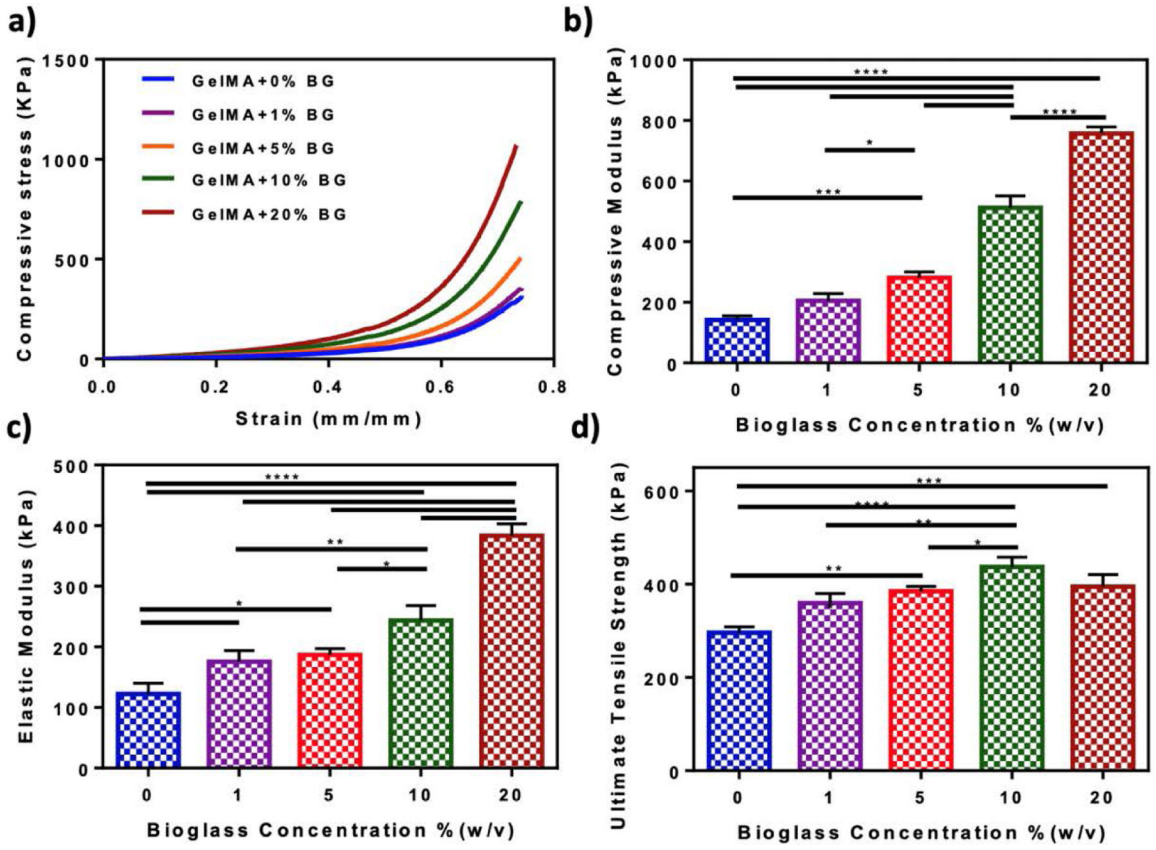

Figure 2. Mechanical characterization of GelMA/BG-5/5 composites.

(a) Representative compressive stress-strain curves **(b)** compressive modulus, **(c)** elastic modulus, and **(d)** ultimate tensile strength of hydrogels synthesized using 10% (w/v) GelMA and varying BG-5/5 concentrations (i.e., 1, 5, 10, and 20%). Data are represented as mean ± SD (*p<0.05, **p<0.01, ***p<0.001, ****p<0.0001 and n ≥ 5).

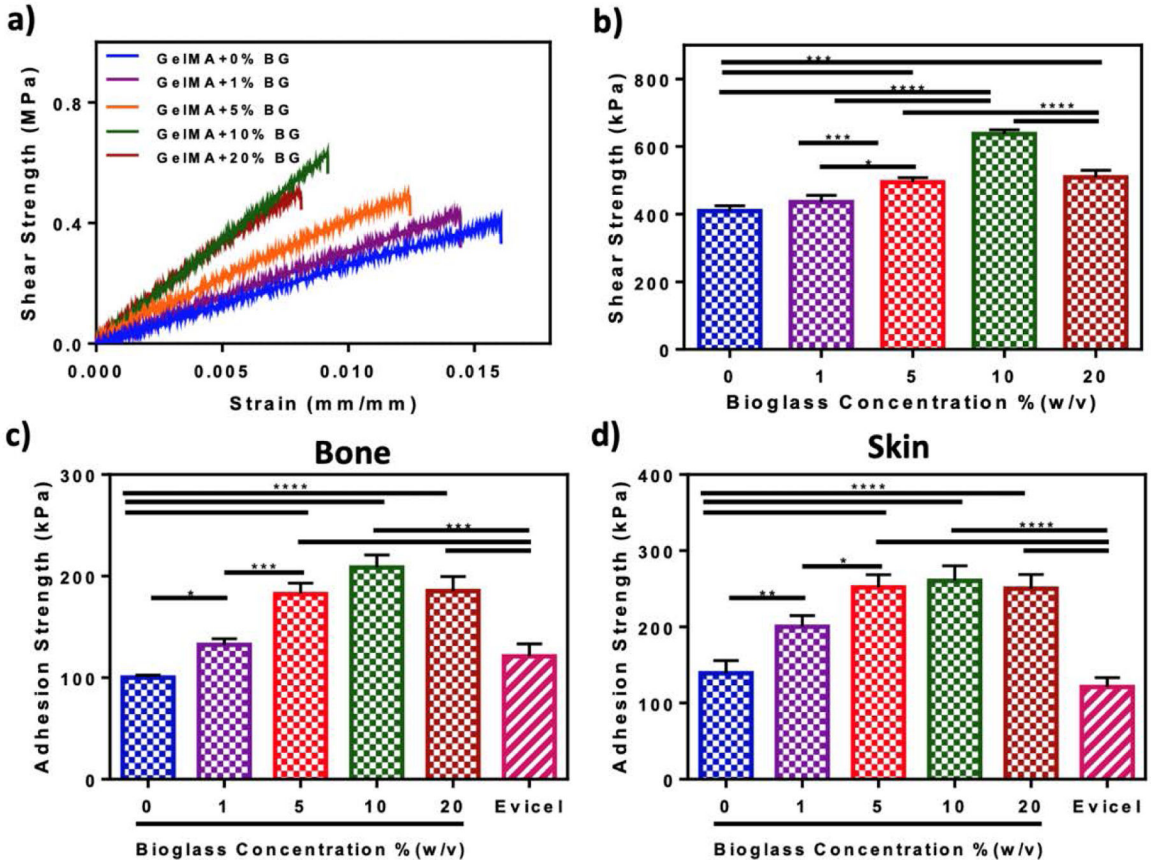

Figure 3. ***In vitro*** **adhesive properties of GelMA/BG composite hydrogels.**

(a) Representative shear strength-strain curves **(b)** shear strength, and **(c-d)** adhesive strength to porcine bone and skin for hydrogels synthesized using 10% (w/v) GelMA and varying BG-5/5 concentrations. Data are represented as mean ± SD (*p<0.05, **p<0.01, ***p<0.001, ****p<0.0001 and n ≥ 5).

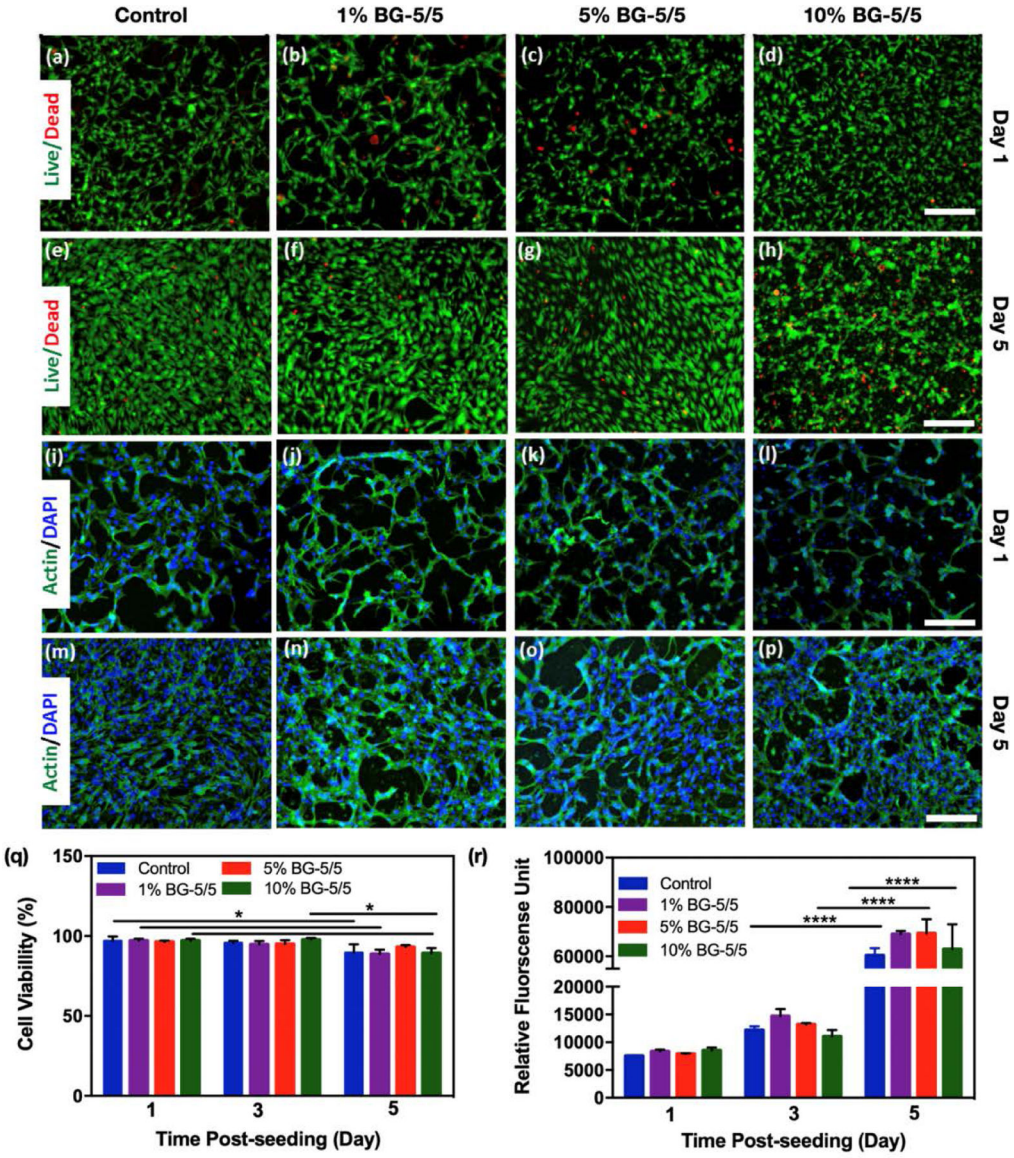

Figure 4. 2D surface seeding of MC3T3-M1 cells on GelMA/BG-5/5 composites.

MC3T3-M1 cells were seeded on the surface of composites synthesized using different concentrations of BG-5/5 (i.e., 0%, 1%, 5% and 10%) and maintained in culture for 5 days. Representative live/dead fluorescent micrographs of cells at days (**a-d**) 1 and (**e-h**) 5 post-seeding. Representative F-actin/DAPI fluorescent micrographs of cells at days (**i-l**) 1 and (**m-p**) 5 post-seeding. Quantification of **(q)** cell viability and (**r**) metabolic activity of MC3T3-M1 cells grown on the surface of composites synthesized using varying concentrations of BG-5/5 at days 1, 3, and 5 post seeding (* $p < 0.05$, ** $p < 0.01$, *** $p < 0.001$, **** $p < 0.0001$). Scale bars = 200 μm.

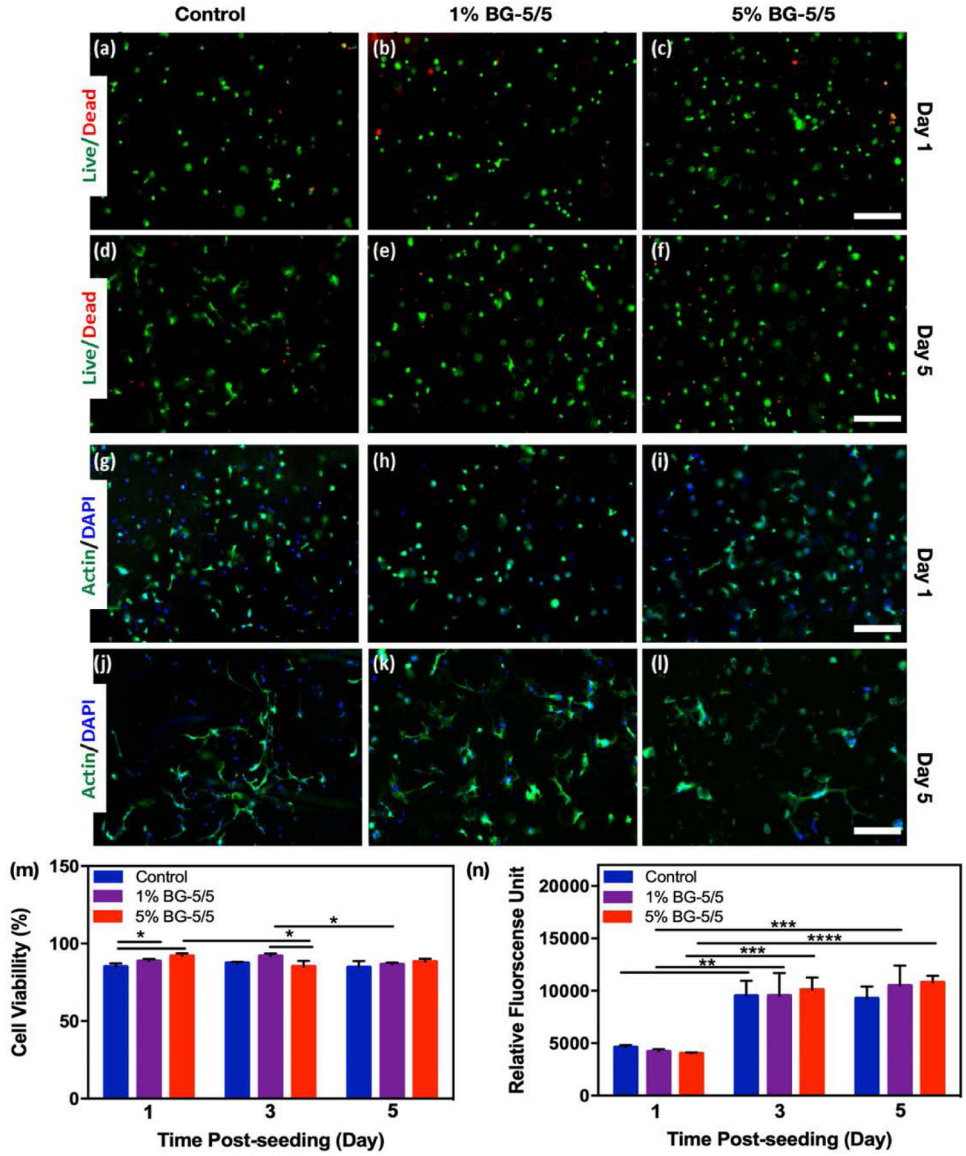

Figure 5. 3D encapsulation of MC3T3-M1 cells in GelMA/BG-5/5 composites.

MC3T3-M1 cells were encapsulated inside composites synthesized using different concentrations of BG-5/5 (i.e., 0%, 1%, 5% and 10%) and maintained in culture for 5 days. Representative live/dead fluorescent micrographs of cells at days (**a-c**) 1 and (**d-f**) 5 post-encapsulation. Representative F-actin/DAPI fluorescent micrographs of cells at days (**g-i**) 1 and (**j-l**) 5 post-seeding. Quantification of **(m)** cell viability and (**n**) metabolic activity of MC3T3-M1 cells grown on the surface of composites synthesized using varying concentrations of BG-5/5 at days 1, 3, and 5 post seeding (* $p < 0.05$, ** $p < 0.01$, *** $p < 0.001$, **** $p < 0.0001$). Scale bars = 200 μm.

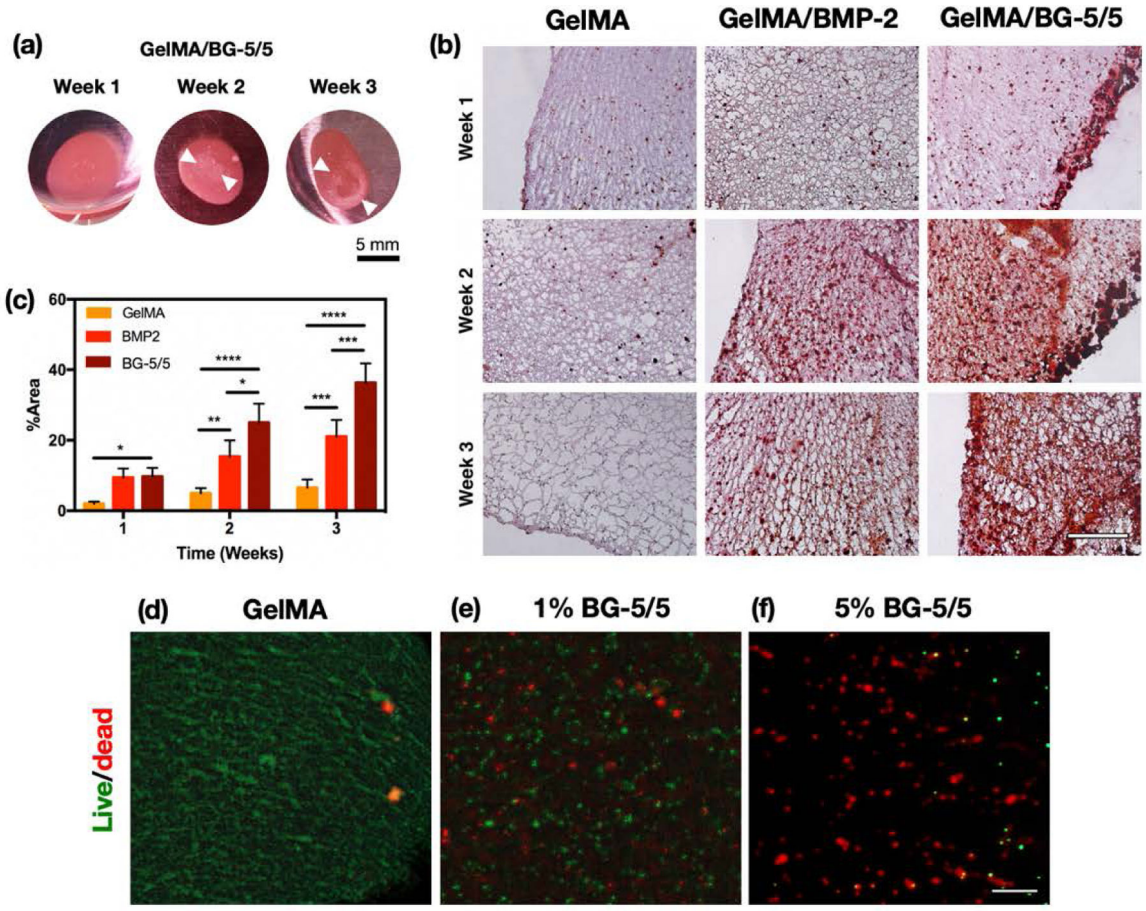

Figure 6. ***In vitro*** **evaluation of osteoinductivity and antimicrobial properties of GelMA/BG-5/5 composites.**

(**a**) Representative images of GelMA/BG-5/5 composites with 3D encapsulated MC3T3-M1 preosteoblasts at weeks 1, 2, and 3 of culture. White arrows indicate the appearance of mineral crystals on the composites. (**b**) Histological evaluation (Alizarin red) of the osteogenic differentiation of 3D encapsulated MC3T3-M1 cells in GelMA, GelMA/BMP-2, and GelMA/BG-5/5 hydrogels at weeks 1, 2, and 3 post-encapsulation (Scale bar = 500 μm). (**c**) Quantitative image analysis of Alizarin Red S-stained micrographs. (*$p < 0.05$, **$p < 0.01$, ***$p < 0.001$ and ****$p < 0.0001$). Representative fluorescent micrographs of the BacLight viability assay. MRSA were grown on (**d**) GelMA hydrogel, (**e**) GelMA hydrogel with 1% BG-5/5, and (**f**) GelMA hydrogel with 5% BG-5/5 (Scale bar = 20 μm).